Automation in Construction 167 (2024) 105664

Contents lists available at ScienceDirect

Automation in Construction

journal homepage: www.elsevier.com/locate/autcon

Road pavement health monitoring system using smartphone sensing with a two-stage machine learning model

Kai Zhao [a,b], Shuoshuo Xu [a,b], James Loney [c], Andrea Visentin [b,d], Zili Li [a,b,*]

[a] School of Engineering and Architecture, University College Cork, Cork, Ireland
[b] Insight Centre for Data Analytics, Ireland
[c] McCurdy Associates, Ireland
[d] School of Computer Science & IT, University College Cork, Ireland

ARTICLE INFO

Keywords:
Drive-by road pavement monitoring
Structural health monitoring
Smartphone sensing
2-stage machine learning

ABSTRACT

Drive-by road pavement monitoring, using smartphone sensing, has faced longstanding challenges in adoption due to low accuracy and limited applicability. This stems from significant uncertainties during data collection in real-world scenarios, making it prohibitively difficult in applying conventional machine learning models to the detection of road pavement anomalies. This paper presents a two-stage machine learning approach that extracts potential anomalies from the dataset and classifies them into four typical road feature categories. Unlike time-series data analysis, this approach transforms time-series into geospatial series, allowing the analysis to be time-independent thereby capable of detecting road anomalies regardless of driving speeds. Additionally, a framework for a road pavement health monitoring system is proposed to collect data, integrate the machine learning engine, and visualise road anomalies. The developed system was tested on two shuttle buses with normal smartphones, which achieved 87% overall accuracy compared against manual inspection.

1. Introduction

Road pavements inevitably deteriorate over time due to environmental corrosion and constant loading. Severely deteriorated road pavements could reduce the comfort of road users, increase the carbon emissions of vehicles [1], and pose safety risks to society [2]. In many countries around the world, the conditions of road pavements are one of the foremost concerns among other infrastructures [3]. However, due to the combined effects of natural deterioration and constant traffic loadings, a growing number of road segments are inevitably degrading, increasing costs on road health monitoring and repairing every year [3,4]. According to the US National Transportation Research groups, driving on pavement needing repair costs each road user US $599 million in 2020 [5]. In Ireland, the asset owner has reported spending over €1 billion in 2021 alone to bring these deteriorated roads up to standard [6].

One of the reasons causing huge costs is that the current road monitoring practices highly rely on conventional specialized equipment methods. For example, 3D reconstructions, as one of the widely adopted road monitoring approaches, rely on the inertial laser profilometers installed on the vehicle and operated by specialists to build road profile models with high resolution to detect road anomalies [7,8]. Even though it provides high precision measurements, its equipment is expensive to own and operate, especially in national road networks, making it impossible to conduct frequent monitoring [4]. Another example is the vision-based approach, which is a compromise of 3D reconstruction by using a camera mounted on vehicles facing towards the road surface to collect geotagged images and image processing techniques, such as texture extraction [9], Canny edge detection [10], to depict road defect features. Compared to 3D reconstruction, it provides a cost-effective solution by having half-automated approaches. However, it is highly restricted to environmental conditions and testing environments, such as rain, shadow, vehicle speed, etc. [11]. Nevertheless, the nature of both 3D reconstruction and vision-based approaches demands extensive labour and often necessitates manual inspections and measurements, incurring high substantial environmental and economic costs. The vibration-based approaches, on the other hand, offer a promising alternative by detecting road anomalies using motion sensors and Global Positioning Systems (GPS) which are much more accessible than inertial laser profilometers and cameras, e.g. ones integrated into smartphones. Synergized with well-trained machine learning algorithms, the vibration-based approaches eliminate human intervention and

* Corresponding author at: School of Engineering and Architecture, University College Cork, Cork, Ireland.
E-mail address: zili.li@ucc.ie (Z. Li).

https://doi.org/10.1016/j.autcon.2024.105664
Received 23 February 2024; Received in revised form 29 July 2024; Accepted 29 July 2024
Available online 17 August 2024

restrictive conditions, significantly reducing the costs and safety risks associated with regular road health monitoring.

Over the past decade, using motion data collected by smartphone sensors to detect road pavement anomalies has been extensively studied. These approaches normally comprise three steps: data pre-processing, anomaly detection, and data post-processing. The data pre-processing plays an essential role in filtering the noise and transforming data to keep data structure compatible with anomaly detection and increase the prediction accuracy. Different filters can be applied in the frequency domain to eliminate these noises. However, research on the features of those noises and approaches to eliminate them shows significant disagreement. For example, for engine noises, Cabral et al. and Rajiv et al. applied a lowpass 3rd-order Butterworth filter with 5 Hz and 4 Hz cut-off frequency, respectively [12,13] while Du et al. considered that engine vibration creates frequencies >30 Hz [14]. However, according to Douangphachanh and Oneyama, accelerations generated by road anomalies most likely have a frequency range between 40 and 50 Hz [15], i.e., any lowpass below 40 Hz will remove the accelerations for road anomalies. For noises such as vehicle turning, lane changing, and acceleration or deceleration, Basavaraju et al. applied an 11th order Butterworth filter with a 3 Hz highpass filter [16] while Zang et al. applied a 0.5 Hz filter [17]. Additionally, the reason why certain filters are applied in the above research has hardly been explained. The lack of research on underlying understanding of noises, however, can lead to elimination of interesting data, thereby significantly reducing the accuracy of anomaly detection stage or even failing to detect the anomalies at all.

Prior to road anomaly detection, the gathered sensor data, as typical time-series, requires to be divided into different time windows with the same time interval as one data point [1,2,18,19]. An anomaly detection approach is then applied to identify the anomalies within each window.

One of the most popular approaches is the threshold-based approach or statistical approach, as the method uses statistical features extracted from z-axis acceleration data [11]. The key to the approach is to determine the proper types and values of threshold to identify desired features, such as amplitudes of the acceleration signal [1,20–22] or standard deviations of windows [23–26]. However, the threshold-based approach is highly sensitive to testing conditions such as vehicles' suspension systems, smartphone placement, various sensors, and mechanical properties [11]. Additionally, due to analyzing using one single value as thresholds, the bidimensional features of acceleration data can be easily ignored. Thus, the method is only capable of detecting simple road anomalies which cause acute vibrations, such as potholes and speedbumps.

In the rapidly advancing era of artificial intelligence, machine learning (ML) approaches have gathered significant attention and extensive research on road anomaly detection. Du et al. [27] and Alam et al. [28] proposed a K-nearest Neighbor (KNN) to detect road bumps and potholes using vibration data. Perttunen et al. [29] and Bhoraskar et al. [19] have both explored the application of Support Vector Machine (SVM), a supervised learning approach, to effectively classify smooth roads and bumpy roads. On the other hand, Pawar et al. have proposed a Neural Network model consisting of two hidden layers and one output layer for a similar road classification task, where the proposed model can reach 94.78% accuracy [30]. Attention has also been paid to classifying different types of anomalies. Dey et al. and Basavaraju et al. proposed a SVM approach to classify potholes, speed bumps, rumble strips, smooth and rough roads with 92% overall accuracy [16,31]. While Silva et al. evaluated several supervised ML approaches, including Gradient Boosting (GB), Decision Tree (DT), Multilayer Perceptron Classifier (MLP), Gaussian Naive Bayes (GNB), and SVM, for classifying road surface distress into bumps and manholes [32]. Although high overall accuracy has been achieved in most of the research, the evaluation on overall accuracy is hard to analyze in the road pavement anomaly problem as this is typical unbalanced datasets where the cases of normal road segments are significantly more than anomalies. With evaluation on just anomalies, such as research by Tai et al. [33] who achieved a precision of 78.5% in pothole detection and by Wu et al. who achieved classification with a precision of 88.5% and recall of 75%, the accuracies are relatively low. Attention has also been paid to using deep learning algorithms, such as recurrent neural networks (RNN) by Maeda et al. [34], and Long Short-Term Memory networks (LSTMs) by Varona et al. [35], which are widely adopted approaches for anomalies detection. However, RNNs and LSTMs, being deep learning algorithms designed to capture dependencies and patterns in time series, are more apt for tasks like sound recognition and irregularity detection in machinery vibrations and require a consistent amount of labelled training data. In road pavement anomalies detection, however, the patterns of the anomalies exhibit a substantial degree of randomness even after noise reduction, which are hard to identify using deep learning models, or at least for limited number of labelled samples.

The most significant obstacle that deteriorates the accuracy of detecting road pavement anomalies is the alignment of sliding windows in the time series data, which serve as samples in training and prediction. These windows are challenging to align with anomalies, as they are either too large (minimizing window features, such as standard deviation) or too small (failing to represent the entire anomaly).

Another limitation of most anomaly detection systems is that the testing environment operates under controlled or partially controlled conditions. For instance, drivers are required to maintain constant or near-constant speeds to avoid variations in data points due to changing speeds. For example, Silva et al.'s approach [32] limited the sampling rate to 50 Hz to minimize the speed effect. Varona et al. [35] distinguish road anomalies from movements of vehicles caused by driver actions. Chuang et al. [36] categorized the data into three speed ranges: <40 km/h, 40 to 80 km/h, and > 80 km/h, to calculate the IRI, respectively. However, this effect is challenging to represent by merely grouping into speed ranges, as the vehicle's speed changes continuously, especially on busy road networks where accelerations and stops occur frequently.

In this research, an innovative road health monitoring system with a two-stage machine learning model is proposed. The approach addresses several key challenges by employing unique methodologies. In the data pre-processing stage, the proposed research delves into the different types of noise sources and proposes an effective filter to remove them. Additionally, instead of using time domain data, the proposed approach converts time series data to geospatial data by adopting GPS locations, eliminating the influence of the speed of vehicles, therefore making the system suitable for community-level implementation. Following data filtering, the first stage model detects the potential anomalies using a Random Forest Classifier (RFC), while the second stage further classifies them into four distinct categories, including normal road windows, large cracks, road bumps and potholes, using a Gaussian Process Classifier. Such a two-stage model significantly outperforms the conventional one-off machine learning models for road pavement surface anomaly detections. To assess its efficacy, comprehensive testing was conducted on a regular bus running in Cork, Ireland, under real-world and uncontrolled conditions.

The introduction section highlights the engineering significance of road pavement surface monitoring, followed by a brief description of the pros and cons of conventional road monitoring methods. The advantages and limitations of peer research in road pavement surface monitoring approaches using smartphone sensing are then listed, highlighting the urgent need to develop comprehensive noise reduction techniques, geospatial data transformation, and a two-stage machine learning approach. The rest of this paper is organized as follows: Section 2 outlines the overall methodology of the proposed approach. Section 3 details the data collection and preprocessing. Section 4 describes the two-stage machine learning model. Section 5 illustrates the results obtained from a real-world implementation. Conclusions are given in Section 6.

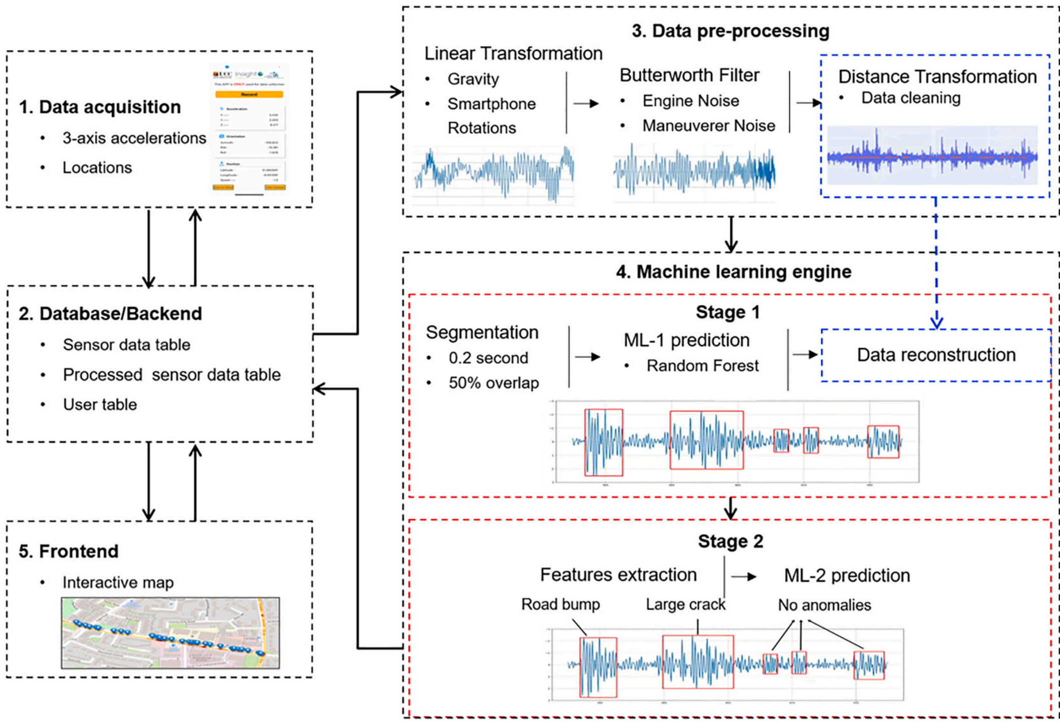

Fig. 1. Workflow of 2-stage machine learning road anomaly detection system.

2. Overview of the road health monitoring system

The proposed approach consists of five distinct steps, comprising data acquisition, data base/backend, data pre-processing, machine learning engine and frontend, as illustrated in Fig. 1.

1. Initial data acquisition involves the capture of motion sensor and location data through smartphones in the first layer of data collection. In this phase, a dedicated smartphone application is developed to facilitate the systematic collection and transmission of data to the cloud.
2. The acquired data is then stored in the cloud, and a backend system has been constructed to manage the data flow effectively.
3. Following data acquisition, the raw data is subjected to a data pre-processing layer, where most of the noises are minimized to a level enabling the identification of anomaly features. Subsequently, the accelerations, presented as time series data, are transformed into geospatial series using polynomial interpolation between every two adjacent GPS coordinates.
4. The machine learning engine consists of a two-stage machine learning model. In the first stage of the machine learning model, a binary classification model employing random forest is trained to classify small segments of the time series into high (positive) and low (negative) vibrations. The segments identified as high vibrations are then reconstructed into larger windows, each potentially containing road anomalies. These windows are further transformed from time series into geospatial series data, with each serving as an anomaly window in the subsequent classification.

In the second stage of the machine learning model, features of anomaly windows are extracted and assembled as samples to for classification using a trained Gaussian Process Classifier (GPC). Four classes are considered in this research, including normal road windows, large cracks, road bumps and potholes. The mean predictions of each sample and associated probabilities are obtained through GPC. 5. In the last step, those results, along with the lengths and severity of the anomalies, are geographically marked on the map according to their GPS information from the first step.

A pivotal difference between the proposed methodology and existing peer research lies in the incorporation of GPS coordinates, which are transformed into geospatial series for calculating the lengths of anomalies as part of the machine learning training and predictions. In contrast, peer research merely employs GPS coordinates for mapping road anomalies. There are two notable advantages of the proposed method over peer research. Firstly, the transformation from temporal data (time series) to geospatial data allows road anomaly lengths or length-related parameters to be one of the features. This proves particularly advantageous in distinguishing anomalies, such as potholes, which generally generate short but intense vibrations over a relatively short period of distance. Secondly, the geospatial series data is characteristic by time independent, enabling the detection of anomalies regardless of the speed of vehicles. Eliminating the need to control vehicle speed during detection enhances the versatility of data collection, facilitating operations in various scenarios, even in city centres where stationary, acceleration, and deceleration events are inevitable.

Instead of detecting anomalies directly from the dataset, a two-level machine learning model is introduced in this research to first extract potential anomalies and subsequently classify them into different categories. Similar to machine learning models for objective detections, the first stage model is designed to pinpoint the potential anomalies, predicting their distances and vibration ranges, shown as red boxes in Fig. 1. The second stage model will concentrate exclusively on those identified samples, classifying them into four classes: normal road segments, large cracks, road bumps and potholes. Thus, the road pavement anomalies can be identified as well as classified. Furthermore, the model provides probabilities for each class, along with information on the lengths and severity of anomalies, aiding in informed decision-making for road maintenance. This is unattainable through conventional one-off machine learning models. Because the training and test sets of such models require them to be homogeneous in terms of sizes or necessitate specific alterations in a user-defined pattern. Thus, such models struggle to focus on anomalies directly, given that road defects appear randomly in lengths and locations. In comparison to one-off machine learning models, the proposed two-level approach can capture and directly focus

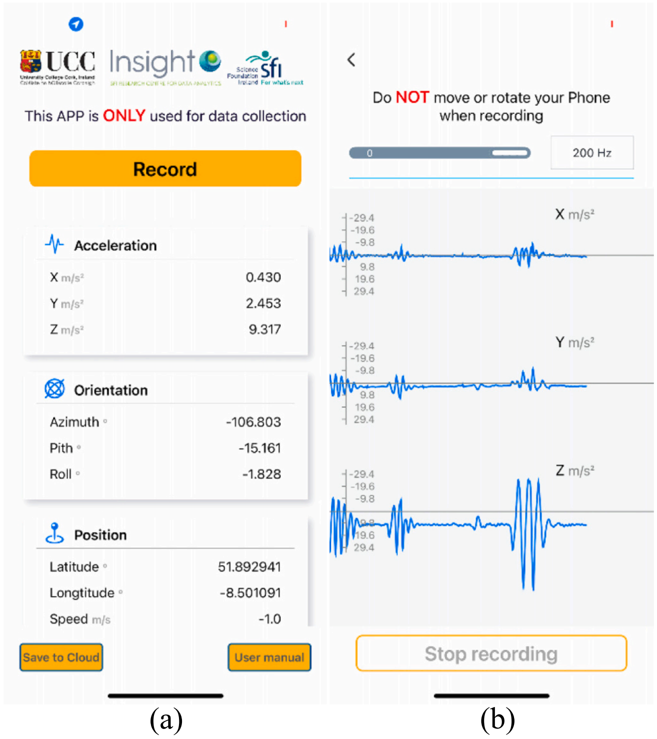

Fig. 2. Smartphone application interface: (a). main page; (b). recording page.

on vibrations of anomalies, increasing the accuracy of features that describe them. Additionally, having lengths as features of the anomaly windows, the proposed approach is more informative and exhibits significantly improved overall accuracy, offering a more comprehensive understanding of road pavement anomalies.

3. Smartphone sensor data collection and processing

It is advised by Ferjani and Alsaif [37] that vibrations of drive-by vehicles induced by road anomalies are largely associated with z-axis accelerations (vertical vibrations of vehicle, as shown in Fig. 2). There is a partial association between x-axis and y-axis accelerations, representing horizontal and longitudinal directions of the vehicle, respectively. To further mitigate the dependency of the rotation of the smartphones, rotation data encompassing pitch, roll and azimuth is recorded. Additionally, the GPS coordinates are also collected to incorporate the spatial locations of the anomalies along with acceleration data.

3.1. Smartphone application development

To collect motion and GPS data, a dedicated iOS-based application was designed to read and upload the data from smartphones to the cloud for further processing. The application was developed through the iOS-based platform, X-code. The SensorManager class enables access to motion sensors, while the LocationManager class is employed to retrieve location data. The default sampling rate of motion sensors embedded in a standard iPhone within the iOS API is 100 Hz. However, the maximum sampling rate can be adjusted to reach up to 200 Hz by modifying the recording time interval. In the application, a customizable sample rate was implemented through a scroll bar. This feature allows for the investigation of the impact of sampling rate variations on the accuracy of road anomaly detection, as illustrated in Fig. 2. This flexibility in sampling rates enhances the adaptability of the application to different scenarios, contributing to a more comprehensive analysis of road anomalies.

The GPS data, on the other hand, is provided by the navigation satellites from the network provider, with maximum sampling rate capped at 1 Hz. Notably, in addition to longitude and latitude data, the GPS provider also provides vehicles' speed and bearing, both of which are leveraged in this research. However, as the reliability of the GPS data is contingent on the quality of the signal, i.e. poor internet connections introduce delays in reflecting the current speed, the vehicle's speed is calculated directly from the longitudes and latitudes.

3.2. Data processing

Among all vibration-based road pavement monitoring approaches, the predominant concern revolves around the impact of noises, which significantly diminishes detection accuracy by generating numerous false positives. Across various research endeavours, a common practice is to develop a data processing module for pre-processing raw data before integrating it into any detection mechanism. However, seldom attention is given to delving into the nature of the noises. In many cases, a trial-and-error approach is employed, resulting in substantial discrepancy among peer research studies when attempting to remove those noises. The absence of such observations hinders the development of more effective noise removal strategies. A comprehensive examination and understanding of noise characteristics are essential for enhancing the accuracy and reliability of road pavement monitoring systems.

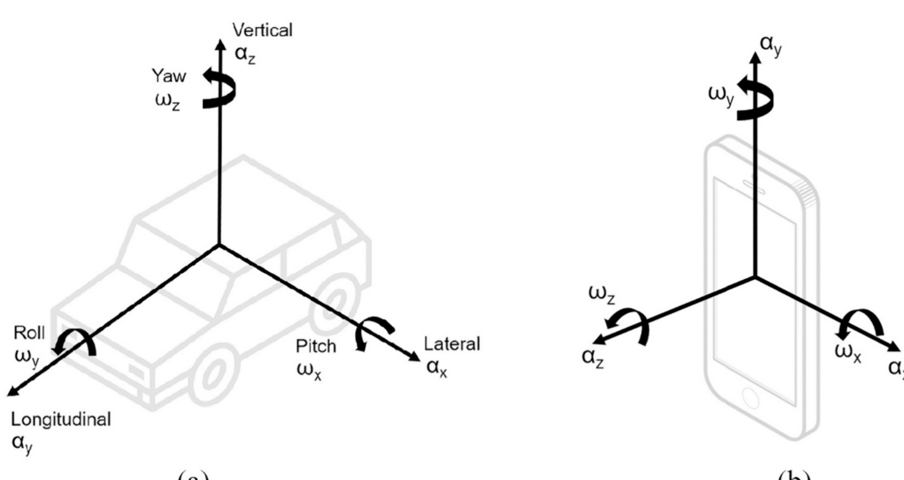

Fig. 3. Linear and angular motion along the axes of a vehicle (a) and a smartphone (b) [4].

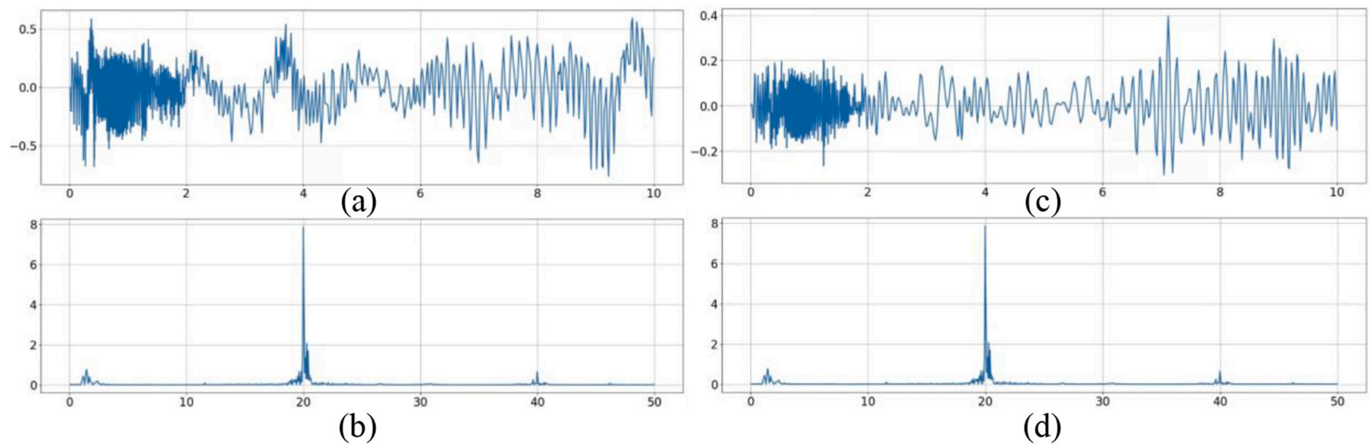

Fig. 4. Time domain and Frequency domain of engine noise before and after filtering by 19 Hz lowpass: (a) raw data, time domain; (b) raw data, frequency domain; (c) filtered data, time domain; (d) filtered data, time domain.

The first type of noise considered in this study is the one caused by the orientation mismatch of vehicle and smartphone, as shown in Fig. 3. Inevitably, during data collection, the orientations of the smartphone do not perfectly align with those of the vehicles, causing accelerations in 3 axes that cannot represent the vehicle's vibrations. This can be removed by transforming linear accelerations along smartphones' axes into linear accelerations along vehicle axes using the transformation matrix in Eq. 2.1. The gravity can then be subtracted from vertical acceleration. The 3-axis accelerations can, thus, represent the orthogonal movement of the vehicles.

$$\begin{bmatrix} Acc_x \\ Acc_y \\ Acc_z \end{bmatrix}_{veh} = \begin{bmatrix} 1 & 0 & 0 \\ 0 & cos\alpha & -sin\alpha \\ 0 & -sin\alpha & cos\alpha \end{bmatrix} \begin{bmatrix} cos\beta & 0 & sin\beta \\ 0 & 1 & 0 \\ -sin\beta & 0 & cos\beta \end{bmatrix} \begin{bmatrix} cos\gamma & -sin\gamma & 0 \\ sin\gamma & cos\gamma & 0 \\ 0 & 0 & 1 \end{bmatrix} \begin{bmatrix} Acc_x \\ Acc_y \\ Acc_z \end{bmatrix}_{dev} \tag{2.1}$$

Where $Acc_{x,y,z}$ are linear accelerations in m/s^2 along 3 axes. α, β and γ are the Euler angles about x, y and z axes, respectively, as shown in the Fig. 3.

Engines emerge as a prominent source generating large vibrations, which the smartphone sensors can easily pick up. In fact, this noise component is relatively straightforward to eliminate as it causes stable and consistent patterns throughout the entire data collection process. It is worth noting that it is advised by [38] that it takes approximately 20 s for the engine and smartphone sensors to be stabilized after engine starts operating. The first 20 s of dataset are, therefore, discarded.

To obtain the frequency range associate with the engine vibration, the analysis focuses on vertical accelerations when the vehicle is either stationary or moving on a smooth road. Following the transformation of data from the time domain to the frequency domain using the Fourier transform, as shown in Fig. 4 (a, b), it becomes evident that the engine's frequency is centred around 20 Hz. Subsequently, a 4th-order Butterworth filter with a 19 Hz lowpass is employed to filter the data. The filtered accelerations, obtained through the reverse Fourier transform, are illustrated in Fig. 4 (c). Comparing this to the raw data shown in Fig. 4 (a), it is apparent that the time domain data becomes smoother after filtering. Additionally, the magnitude of the frequency at 20 Hz in the frequency domain is significantly reduced, as observed in Fig. 4 (b,

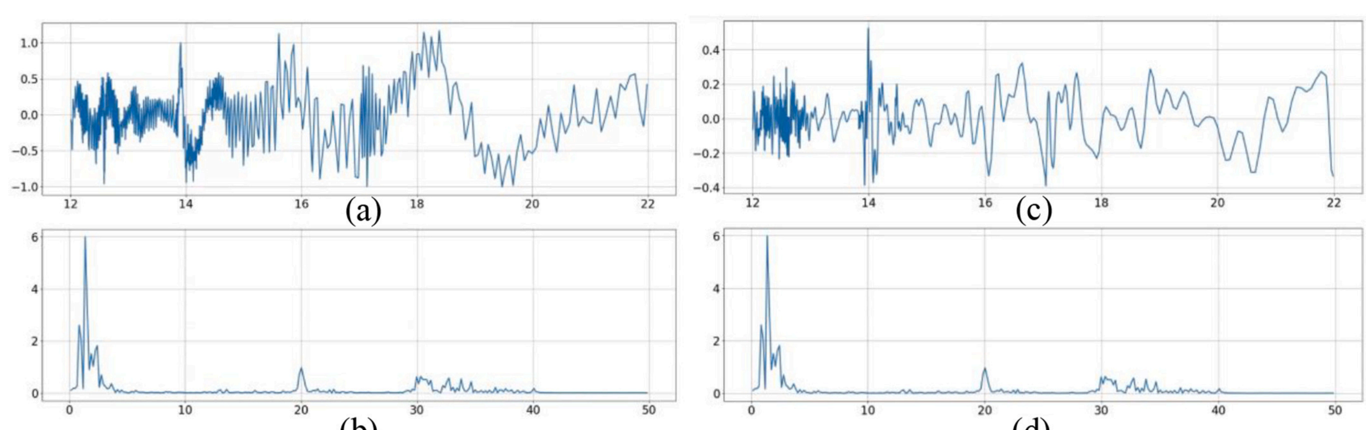

Fig. 5. Time domain and Frequency domain of vehicle acceleration before and after filtering by 3.5 Hz highpass: (a) raw data, time domain; (b) raw data, frequency domain; (c) filtered data, time domain; (d) filtered data, time domain.

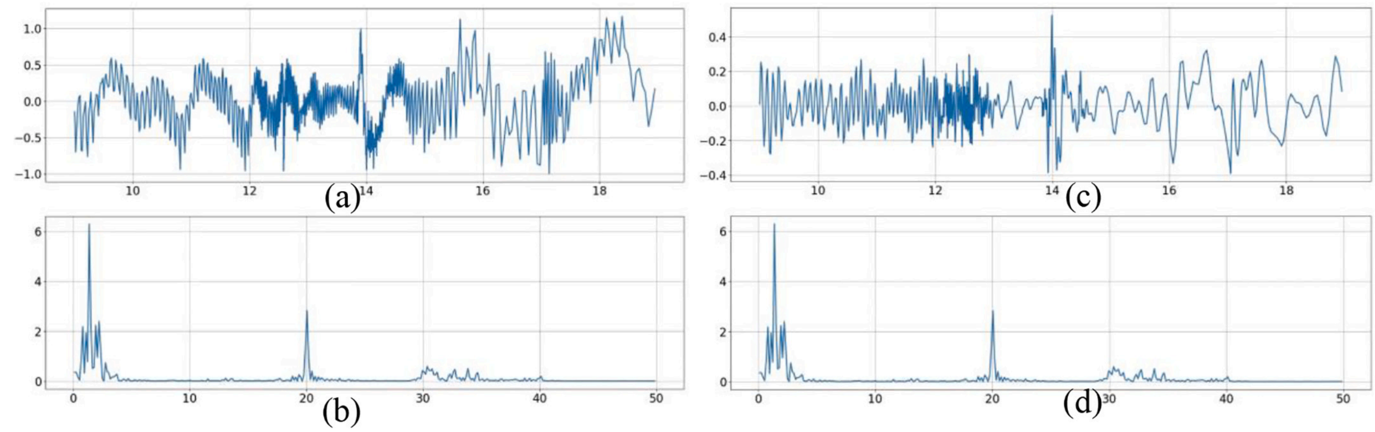

Fig. 6. Time domain and Frequency domain of turning noise before and after filtering by 3.5 Hz highpass: (a) raw data, time domain; (b) raw data, frequency domain; (c) filtered data, time domain; (d) filtered data, time domain.

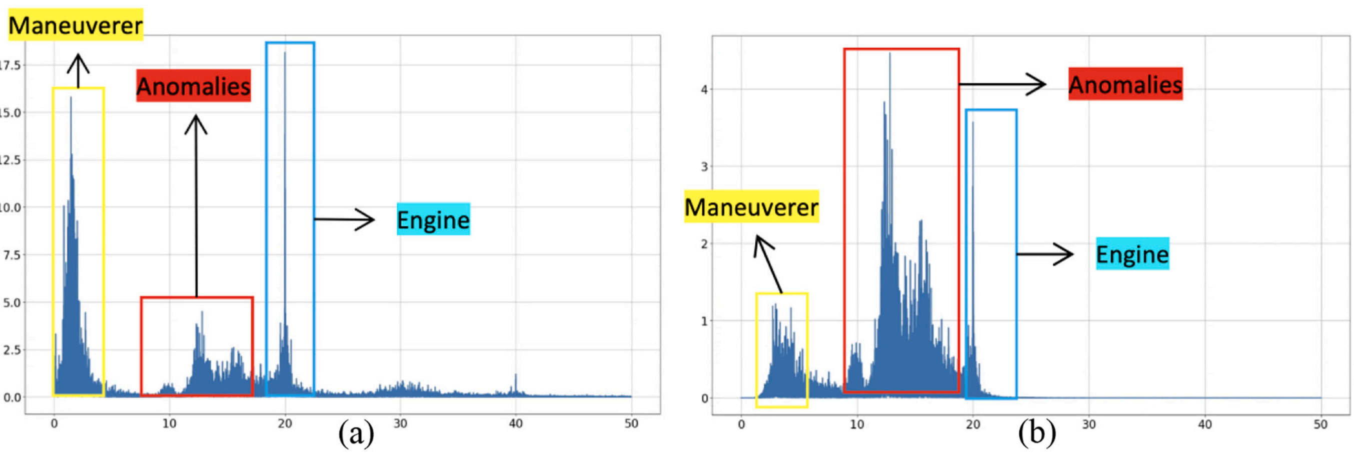

Fig. 7. Frequency domain of raw and filtered data: (a) raw data; (b) filtered data by bandwidth 3.5 Hz – 19 Hz.

d). However, it is important to note that the acceleration caused by the engine cannot be entirely eliminated using the Butterworth filter, as evidenced by the persistence of the spike in the frequency domain. The primary objective of noise removal is to diminish the dominance of noise to the extent that vibrations caused by road anomalies become significant enough to be identified. This phenomenon will be illustrated in Fig. 7.

Drivers (e.g. swerving, turning, and vehicles' accelerations or decelerations) are another source of noise that can significantly compromise the dataset. Similar investigative procedures are applied to address those noise sources. Fig. 5 shows the time domain and frequency domains of vibration data when the vehicle accelerates. It can be seen that the frequency of the noise is located around 3 Hz. To eliminate this, a 4th-order Butterworth filter with a 3.5 Hz highpass is applied. The skewing effect of the time domain data due to acceleration, Fig. 5 (a), is flattened, Fig. 5 (c), after filtering. The removal of vehicles' acceleration-induced noise enhances the prominence of accelerations caused by other sources. Similarly, a frequency of 3 Hz is observed during vehicle turning, as shown in Fig. 6 (a, b). This can also be eliminated using the same filter as vehicle accelerations. Filtered results in Fig. 6(right) underscore the effectiveness of the filtering process. Deceleration and swerving show similar effects with acceleration and turning. Due to redundancy with the preceding content, further elaboration is deemed unnecessary.

Noises along the x-axis and y-axis are also investigated. Distinct differences exist in vibrations across the three axes. For instance, vehicle acceleration and deceleration predominantly induce vibrations along the vehicle's moving direction, i.e., the x-axis. Conversely, turning and swerving predominantly cause significant vibrations along the y-axis. Despite these variations in the power of different vibrations, the frequencies they generate remain consistent. Therefore, identical filters are applied to both the x-axis and y-axis to mitigate these noises effectively.

The efficacy of the filters is assessed on road pavement with anomalies. The overall frequency domain is shown in Fig. 7 (a), and the frequency domain after 3.5 Hz to 19 Hz bandpass filtering is shown in Fig. 7 (b). It can be seen that the frequency range of vibrations induced by the engine is observed above 20 Hz, those resulting from drivers' maneuvers are below 4 Hz, and vibration induced by road anomalies lies within around 5 Hz to 18 Hz. Additionally, the power of the frequency of anomaly vibrations tends to be overshadowed by maneuvers and engine vibrations, creating difficulties in accurately extracting anomaly features. Following filtering, it becomes apparent in Fig. 7 (b) that the vibrations caused by anomalies become more significant compared to the pre-filtered state.

In the last step of the data processing, filtered data are transformed into geospatial series from time series, as shown in Fig. 8, for data processing after first-level machine learning model prediction. The key to this step is to label each vibration point with geographic coordinates and calculate its accumulative distance the journey's starting point using the Haversine formula.

It is important to note that the maximum sampling rate of commercial Global Navigation Satellite Systems is 1 Hz while the sampling rate of the sensors in this research is 100 Hz. Consequently, the vibrations can only be labelled with locations every 1 s, aligning with the

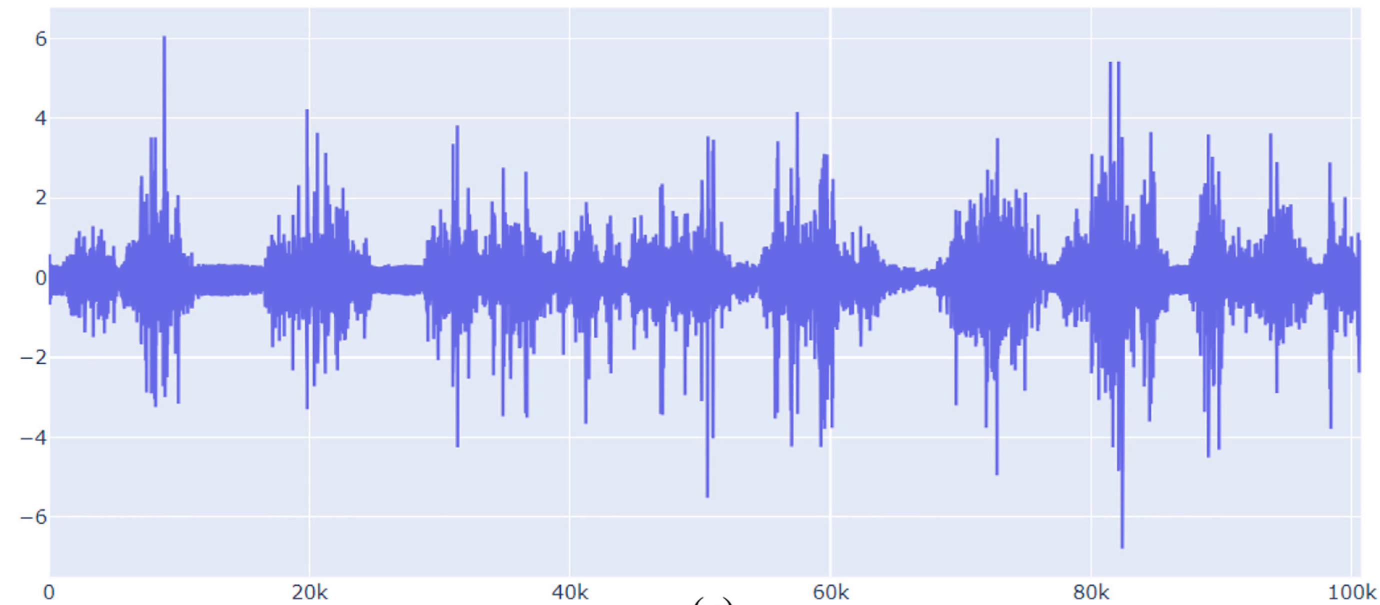

(a)

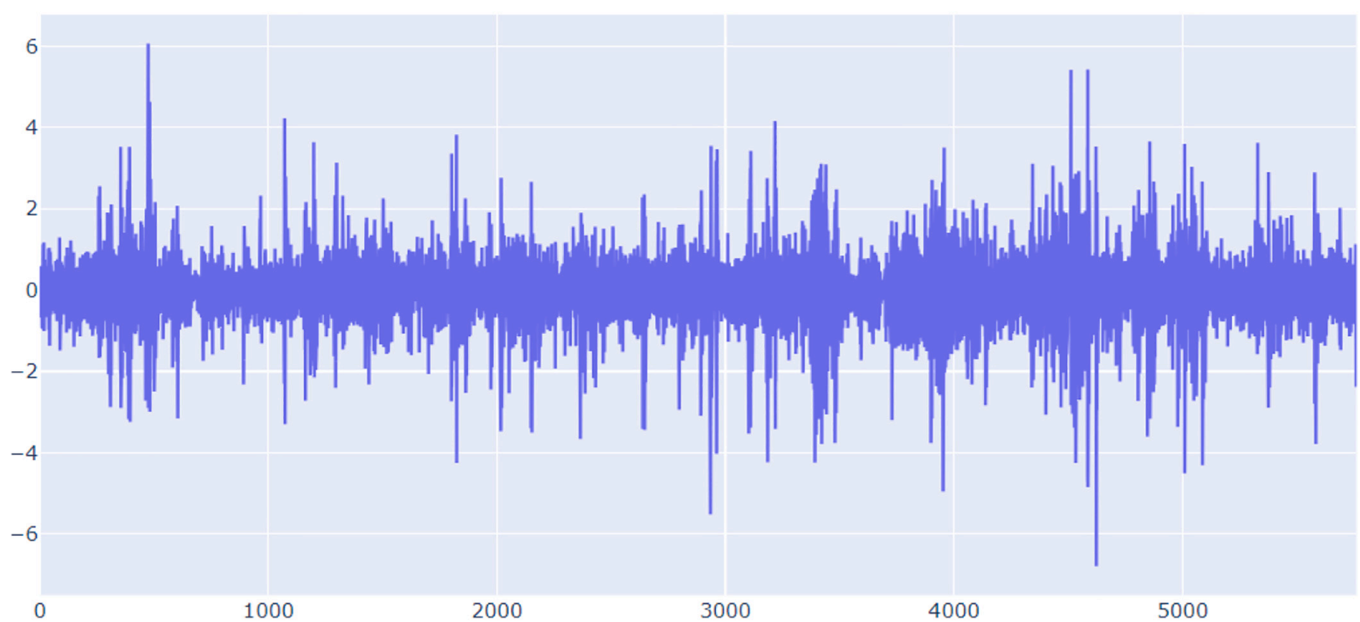

(b)

Fig. 8. Transformation from time-series to geospatial series: (a) accelerations vs time; (a) acceleration vs accumulative distance.

satellite system's sampling rate. To address this discrepancy, the remaining 99 coordinates within each second are approximated through polynomial interpolation based on the average speed of two adjacent coordinates. This average speed is estimated to be approximately equal to the Haversine distance between the two points, see Eq. 2.2. As shown in Fig. 9, along the geospatial axis, vibration data points and their corresponding locations are distributed polynomially based on the average speed. The distance of each point from the starting point A is then calculated using the Haversine formula, providing a coherent representation of the spatial distribution of vibrations over time.

$$H = sin^2(\Delta\varphi/2) + cos\ \varphi1 \cdot cos\ \varphi2 \cdot sin^2(\Delta\lambda/2) \tag{2.2}$$

Noises caused by GPS errors and smartphone sensor inaccuracy should be paid equal attention. Inevitably, signal blockages or being outside signal coverage during data collection can lead to location jumping or loss of data points, resulting in unrealistic large speeds in subsequent calculations and a reduced number of vibration data points. Moreover, sensor inaccuracies are prevalent in most smartphones; for instance, with a pre-set sampling rate of 100 Hz, it was observed that 100.7 data points were collected using an iPhone 13. Such error can be accumulated to a significant error if the data is collected for a long time. The most effective approach to mitigate these errors is identifying and eliminating suspicious data during collection. For GPS errors, a threshold of 80 km/h is set to identify GPS jumps every 2 s. This approach aligns with the intended use for buses operating within city

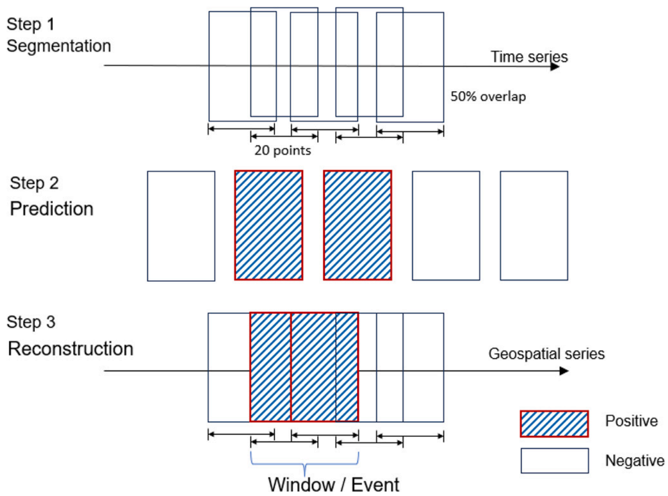

Fig. 9. Workflow of the first stage machine learning.

limits where speed limits are typically below 50 km/h. Regarding sensor inaccuracies, data points exceeding 100 every 2 s are removed. Thus, while minimizing data loss, the errors of sensor inaccuracies are avoided from accumulating.

4. Two-stage machine learning model for road anomaly detection and classification

4.1. Stage-1 machine learning model

The primary objective of the first stage machine learning model is to detect any potential road pavement anomalies using the vibration time series dataset. This concept is similar to machine learning models for objective detection in 2-dimentional datasets, such as, You Only Look Once (YOLO). However, the proposed approach opts for training with 1-dimensional datasets due to the nature of our problem. Fig. 9 shows the procedure adopted to train the machine learning model.

After being pre-processed, the entire dataset is partitioned into small windows. To ensure the model is trained to have enough sensitivity to detect anomalies with a short period of length/time, segments should have a small number of data points. On the other hand, if the lengths of the segments are too short, one may fail to capture and describe the features of the anomaly adequately. In this context, a window of 20 data points with 50% is considered to be capable of detecting any road anomalies that are longer than 0.1 s.

Subsequentially, features are extracted from each segment to serve as samples for training and testing the first machine learning model. Specifically, the standard deviation, mean of the absolute values and skew of each segment are computed and utilized as features. Each sample is manually labelled. The data is then divided into train and test sets. A binary random forest classification model is fitted in the training set. We applied a grid search approach to the hyperparameter selection.

In the final step, segments of the test set that are predicted as consecutive positives are aggregated and reconstructed into windows that contain the whole vibration events. Subsequently, those windows can then be transformed into geospatial series using labels from the data processing layer. The visualization of the results is shown in Fig. 10, where the rectangles' bases represent the length of the anomaly, and the height corresponds to the range from the minimum to the maximum accelerations within them.

The challenge of the 2-stage machine learning model is that the prediction error of the first level model can be inherited by the second stage, thereby affecting the overall accuracy of the model. Specifically, the errors that can be inherited are limited to the false negatives, i.e. the model fails to detect the true anomalies. The false positives, on the other hand, can be treated as one class in the subsequent model. If the recall of the model is or is close to 100%, the error associated with false positives will not be inherited. This can be achieved by adjusting the model's sensitivity ensuring that any ambiguous events are marked as positive.

The conventional evaluation of the classification task is to use a confusion matrix to compare all test labels with predicted labels. However, in the context of road pavement anomaly detection, this evaluation approach describes the accuracy of the segments rather than whole anomaly events. It has been observed that the majority of the false negatives result from misalignment for the same events, thereby misjudging the model's accuracy. Therefore, for the first stage model, the confusion matrix for the events was considered, i.e. it marked as true positives as long as there were overlaps in each window.

4.2. Stage-2 machine learning model

Anomaly-type classification is achieved through the second stage of the machine learning model. By calibrating each window with anomalies identified by manual inspections, the windows are labelled into four categories: normal road, large cracks, road bumps and potholes. It is

Table 1
Features considered in the presented study.

Features	Geospatial domain
Mean	3
Standard derivation (SD)	3
Mean absolute derivation (MAD)	3
Crest Factor (CF)	3
Mean absolute value (Mean(Abs))	3
Root Mean Square (RMS)	3
Maximum Peak to Peak (P2PMax)	3
The Signal Magnitude Area (SMA)	1
Length	1
Slenderness ratio	1
Hump parameter (HP)	1
Total	25

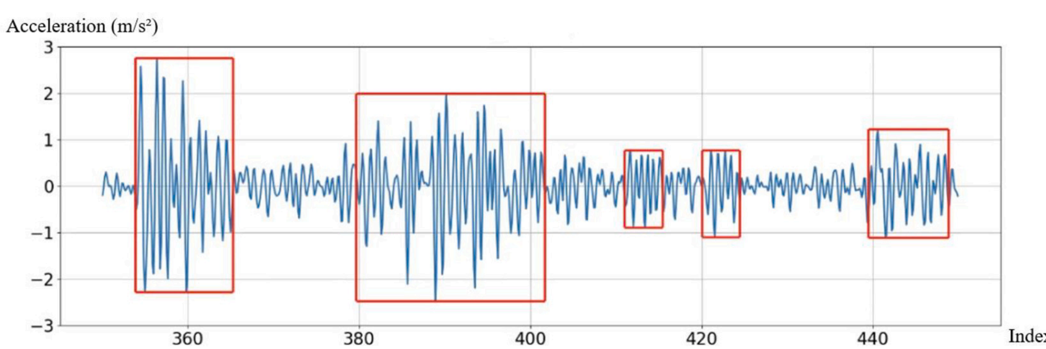

Fig. 10. Visualization of the first stage machine learning model.

Fig. 11. Data acquisition routes and smartphone placements.

worth noting that during data collection and manual inspections, small cracks often induce limited vibrations, easily covered by other vibration sources. Nevertheless, small cracks often received minimal attention during road maintenance, as they neither indicate structural damage nor generate significant vibrations that compromise road user comfort. Additionally, road patches exhibit vibration patterns similar to road bumps and are classified as road bumps, effectively excluding them from the category of road anomalies. Such categorization provides a more refined understanding of the different types of anomalies present in the dataset.

Feature extraction is essential to train machine learning models as unrelated features could deteriorate the accuracy and increase the computational cost. The features that can describe time series data can be extensive, encompassing aspects from both the geospatial and frequency domains for all three-axis accelerations. The features considered in this research are outlined in Table 1. In addition to standard features, three additional ones were specifically implemented for road pavement anomalies detection: lengths, slenderness and hump parameters. It is observed that different types of road anomalies show distinct lengths or height/length ratio (slenderness). For example, potholes typically have a very high height/length ratio as they cause large vibrations in a very short period of time. Whilst the hump parameters are created just for distinguishing humps from other types of anomalies. Humps, which are typically road patches or speed bumps, also cause large vibrations but should be excluded from the road anomalies. When hitting a road hump, vehicles are forced to go up, generating large positive accelerations. On the contrary, normal road anomalies have concave surfaces, causing large negative accelerations. The hump parameter is a value that describes whether the vibration in a window has a high positive value for hump, a low negative value for severer road anomalies, or 0 for relatively low vibrations.

To identify the most relevant features from Table 1, this research employs the mean decrease in impurity (MDI) based on random forest analysis. This method calculates the average decrease in impurity over all trees in the forest, providing a measure of the importance of each feature in making accurate predictions across all trees in the ensemble. Features with a higher mean decrease in impurity are considered more important because they contribute more to the overall reduction in impurity and, consequently, to the model's predictive power. However, the mean decrease in impurity tends to be biased towards numerical features due to the numerical thresholds of splitting criterions. Additionally, for highly correlated features, the importance scores may be spread across them, leading to a dilution of the importance of individual features.

On the other hand, the Self-Organizing Map (SOM) is an unsupervised machine learning algorithm that uses artificial neural networks. By preserving the topological relationships of the input data, similar input samples are attracted and self-organizing to specific regions. Visualizing the weights of each feature can provide valuable insights into the feature importance and feature correlations. Combining SOM with MDI, the most relevant features for the classification task are selected, ensuring a comprehensive understanding of the features that significantly contribute to the model's accuracy.

The classification model for the second stage is trained using a binary Gaussian Process Classification (GPC) model. The Gaussian Process is a stochastic process model that defines a distribution over functions, typically Gaussian, to capture the uncertainty associated with predictions. It is a non-parametric model particularly suitable for small sample models where uncertainties are inherited. For classification tasks based on the Gaussian Process, it provides a probabilistic classification, where the test predictions take the form of class probabilities.

Assuming training dataset $\mathbf{X} = \{x_i\}$ with label $y_i \in \{-1, +1\}$ for binary classifications. The goal is to model the probability $p(y_* = +1 | x_*, \mathbf{X}, y)\}$. Assuming y follows a Gaussian prior with 0 mean and kernel specified covariance $k(x, x')$ on a latent function f, namely nuisance function, that is

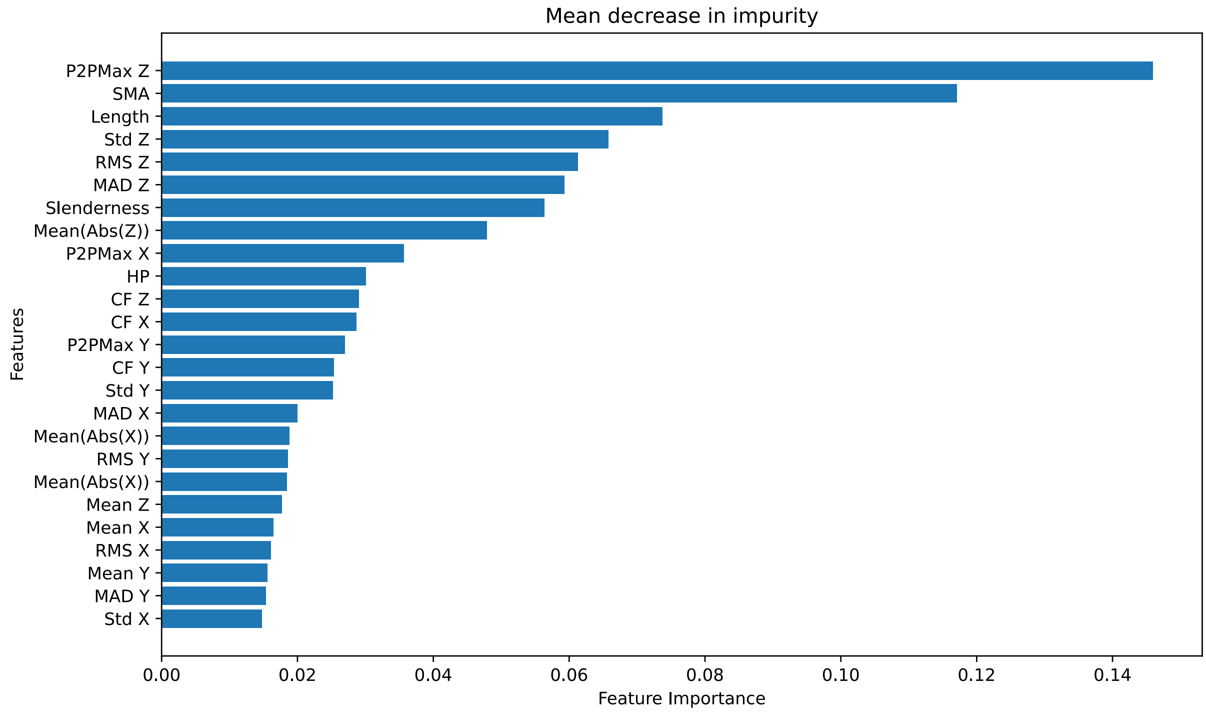

Fig. 12. Mean decrease in impurity over 25 features.

$$f(x) \sim \mathscr{G}(0, k(x, x')) \tag{2.3}$$

The values of the latent function are then passed to a logistic link function, see Eq. 2.4, to the probabilistic classification to obtain class probability $\Phi(x) = \lambda(f(x))$.

$$\lambda(z) = (1 + e^{-z})^{-1} \tag{2.4}$$

The likelihood function of the observed labels y given the latent function $f(x)$ is therefore written as

$$p(y_i|f(x_i)) = \Phi(y_i f(x_i)) \tag{2.5}$$

By Bayes' theorem, the posterior over the latent variables is given by $p(f|X,y) = p(y|f)p(f|X)/p(y|X)$. Unlike Gaussian Process Regression, which assumes the posterior as a Gaussian, the posterior of the latent function f is not Gaussian as the prior goes through a link function. In this case, a Laplace approximation is applied to find the posterior distribution, namely to find the maximum a posterior (MAP) estimate, $\hat{f} = argmax_f\, p(f|\mathbf{X}, \mathbf{y})$. This is obtained by maximizing the log posterior, written as

$$log\, p(f|\mathbf{X}, \mathbf{y}) = log\, p(\mathbf{y}|f) - \frac{1}{2} f^T K^{-1} f - \frac{1}{2} log\, |K| - \frac{n}{2} log\, 2\pi \tag{2.6}$$

The optimal hyperparameters are determined when the MAP is reached. However, to avoid local optimal, it is required to run several iterations during MAP optimization.

The kernel of the GPC, as the most essential part of the model, utilized the most popular choice for GPC, the Radial Basis Function (RBF) kernel, also known as the squared exponential kernel. The RBF kernel is characterized by its ability to capture smooth and continuous functions, as the latent function *f(x)* is assumed to be a smooth function that varies across the input space. As the only hyperparameters in the RBF kernel, the length scales allow to capture the smoothness along each axis. If the length scale is small for a particular dimension, the RBF kernel will be sensitive to variations along this dimension. As there are multiple features to classify the road pavement anomalies, the length scales are a vector with the same number of the dimensions as the features. Additionally, in this research, a constant kernel is multiplied with the RBF to optimise its mean. Thus, the whole kernel is written as

$$k(x_i, x_j) = Cexp\left(-\sum\nolimits_{d=1}^{D} \frac{d(x_i, x_j)^2}{2l_d^2}\right) \tag{2.7}$$

Where C is the constant kernel, D is the number of dimensions and l_d is the length scale for the d-th dimension.

It is important to note that a large length scale means low sensitivity to variations along that feature. This can be caused by either low relativity of that feature to the labels or inadequate observed points, leading to high uncertainties. On the contrary, a low length scale shows high sensitivity to variations, exhibiting high accuracy in the training set, potentially causing overfitting. The hyperparameters for GPC, therefore, require to be evaluated through balancing the accuracy from both training and test sets.

5. Performance evaluation

5.1. Data collection and processing evaluation

The iOS application was installed on two iOS smartphones, iPhone 11 and iPhone 13, to test the sensors' stability across different smartphone models and avoid potential hardware-induced errors. Vibrations and GPS coordinates were collected at sampling rates of 100 Hz and 1 Hz, respectively. To validate the robustness of the data, the collection process occurred along two different routes, involving two distinct types of buses: the minibus Mercedes Sprinter Traveliner and the two-deck bus Volvo B9TL, as illustrated in Fig. 11.The smartphones were securely affixed facing forward under the front seat on the bus lower deck, positioned as close to the vehicle's suspension system as possible for optimal data capture.

The experiment routes comprise various road conditions, including flat stretches, slopes, sharp turns, well-maintained roads, road bumps, and anomalies such as potholes. The routes are located in Cork, Ireland, covering approximately 6 and 5 km respectively, as shown in Fig. 11. Given that the buses encountered multiple stops, starts, and unexpected driving maneuvers as they entered the city centre, the data collection occurred under entirely uncontrolled conditions. Importantly, the driver

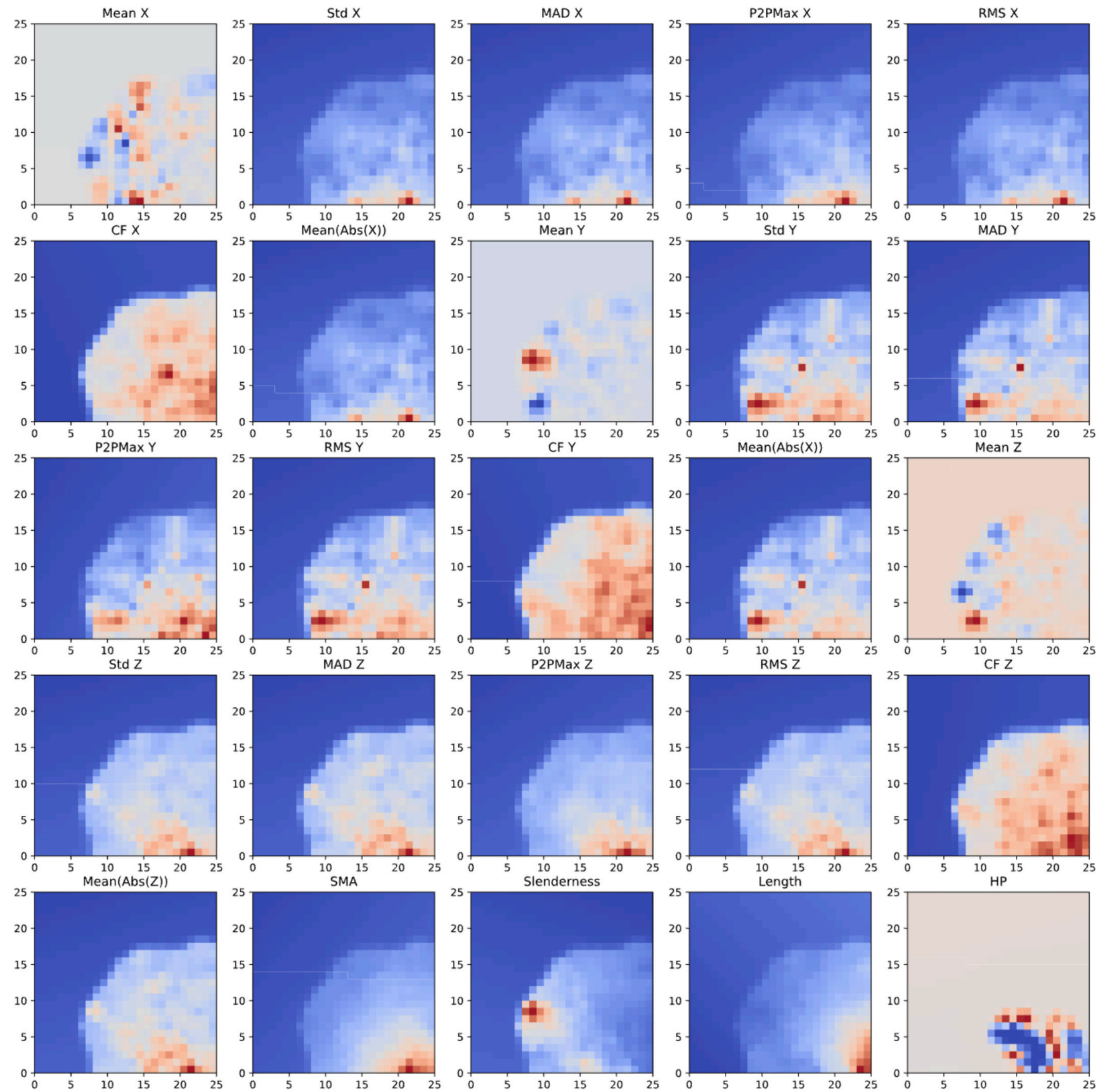

Fig. 13. SOM weight maps on 25 features.

was not informed about the experiment to ensure the authenticity of the data collected. This real-world, uncontrolled setting allows for a robust evaluation of the proposed methodology under diverse and dynamic conditions.

On two routes, a total of 227,575 data points were collected for each axis of acceleration, while 2243 data points were recorded for GPS coordinates. To account for the stabilization period of the engine and GPS upon starting the journey, the first 30 s of data were discarded. Additionally, 20 s of unavailing data, corresponding to parking maneuvers, were excluded before concluding the journey. Subsequently, the trimmed accelerations were cleaned to eliminate sensor inaccuracy and GPS errors and matched with GPS coordinates according to their respective time stamp. The remaining 224,100 accelerations for each axis are then filtered and transformed to geospatial series for second stage ML training and prediction.

5.2. Evaluation on Stage-1 machine learning model

For the first stage machine learning model, by dividing accelerations into segments with 20 data points and 50% overlap, 22,306 segments are generated and labelled with potential anomalies and normal segments. The features, including mean absolute values, standard derivation and skew, are extracted from those segments, forming 22,306 samples. Those samples were randomly divided into 80% for training and 20% as test set.

The training set was then used to fit a RFC model, while the test set was employed to evaluate the model. The depth in the model was selected through hyperparametrisation. A particularity of this

Table 2
GPC training results.

		80% of all datasets				Mercedes Sprinter			Volvo B9TL		
		Precision	Recall	Precision		Precision	Recall	Precision	Precision	Recall	Precision
Training set	Normal road windows	0.92	0.92	0.95	Test set	0.84	0.84	0.86	0.91	0.94	0.92
	Large cracks	0.92	0.92	0.90		0.80	0.80	0.76	0.76	0.76	0.76
	Road bumps	1.00	1.00	0.90		1.00	1.00	1.00	0.83	0.62	0.71
	Potholes	0.80	0.80	0.80		1.00	1.00	1.00	0.75	0.75	0.75
	Overall accuracy			0.92				0.88			0.86

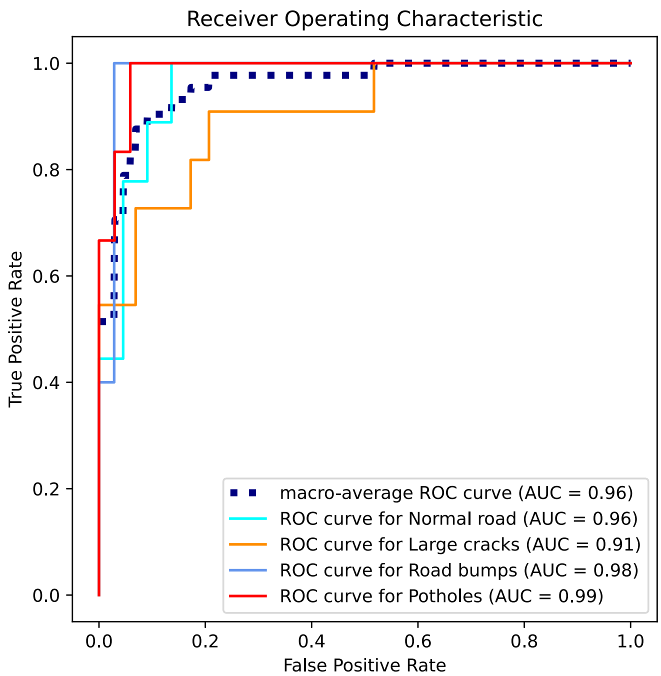

Fig. 14. Receiver Operating Characteristic and Area under Curve (AUC) of GPC model.

application is that the primary objective of the first stage is to have the highest recall or a minimum number of false negatives rather than optimizing the overall accuracy in order to prevent errors from inheriting to the second stage. By balancing the overfit and recalls on training and test set, the optimal depth of 5 is selected.

The validation for the RFC is also conducted in terms of events, as illustrated in Section 2.3, involving the reconstruction of constituent segments into windows and assessing overlaps with labelled data. In the test set, after reconstruction, out of 323 true events, 333 events were predicted, resulting in 0 false negatives. Those windows were then converted from time series to geospatial series so that the accelerations could be time or speed independent, thereby used as features in the stage-2 model.

5.3. Stage-2 machine learning model evaluation

From the first stage machine learning model, 333 windows were predicted as potential road pavement anomalies from 22,306 segments. The features listed in Table 1 were then extracted from these windows for the second stage training and prediction. A feature importance analysis was conducted to identify the most relevant features for the stage-2 model training.

As shown in Fig. 12, the importance of features using the mean decrease in impurity is predominantly associated with those linked to z-axis accelerations. Some features, however, exhibit similar importance levels, resulting in difficulty in selection. Additionally, the features' correlations are complex to observe within MDI, introducing potential issues for highly correlated features.

Table 3
Trained hyperparameters of GPC model.

	Class 1	Class 2	Class 3	Class 4	
Mean	11.7	4.42	6.1	6.75	
L1	7.1e3	8e3	1e5	405	SD
L2	1.52	0.895	2.4e3	2.74	P2PMax
L3	1.2	0.278	3.0e3	0.956	Mean Abs
L4	1e5	1.9e4	1e5	1e4	SMA
L5	1.86	1.14	1e5	1.41	Slender ratio
L6	1e5	1e5	14	2.9e4	Length
L7	1e5	1.06	0.509	9.3e3	Hump factor

A SOM was trained using the Gaussian neighbourhood function with all 25 features, structured in a 25 by 25 grid. The weights of each layer (feature) were visualized on the map to illustrate their patterns. As shown in Fig. 13, it can be observed that the standard derivations, mean absolute derivations, and root mean square of all three axes values exhibit identical patterns, indicating significant correlations between them. Finally, by removing small importance features shown in Fig. 12, P2Pmax, SMA, length, STD, slenderness, length, mean absolute value and hump parameter were ultimately selected to be trained for the next classification task.

Before training and prediction in the second stage, 333 windows were labelled into four categories, including normal road windows, large cracks, road bumps and potholes. Samples were then divided into 80% training and 20% test set. GPC was fitted on the training data, as described in the previous section. For the RBF kernel, there are 8 hyperparameters for each class, including the mean of the RBF and 7 length scales for each feature. The overall accuracy of the test set was achieved at 88% as shown in Table 2.

The accuracy is also evaluated through the Receiver Operating Characteristic (ROC) curve, as illustrated in Fig. 14. The areas under the ROC curve (AUC) for each class are all close to one, indicating a good performance for the model. This analysis further validates the effectiveness of the classification model in distinguishing between different classes of road pavement anomalies.

Observations can also be seen from the hyperparameters of the trained GPC model, as shown in Table 3. Aside from the mean values for each kernel, the length scales indicate the relativity of the features to the corresponding class, i.e. low values indicate high sensitivity and vice versa, noting that the 1e5 is the maximum length scale defined before training the GPC model.

It can be observed that the normal road windows (Class 1) are largely determined by the peak of the maximum to minimum value (P2PMax), mean absolute value and slenderness of the windows. Other features have small impact on predicting this class. Large cracks are predominantly related to the mean absolute values, P2Pmax, slender ratio and the hump factor. Road bumps are associated with the hump factor and the length of the windows. It is common sense when vehicles run over a road bump or anything higher than regular road pavement; they will cause instant large positive accelerations, precisely described by the hump factor. On the other hand, the lengths of the road bumps can vary, as patching on the road is also part of the road bump category, resulting in relatively low sensitivity to the feature of length. For the potholes, it normally causes short but intense vibrations over a short period of length, causing accelerations with high P2PMax and standard

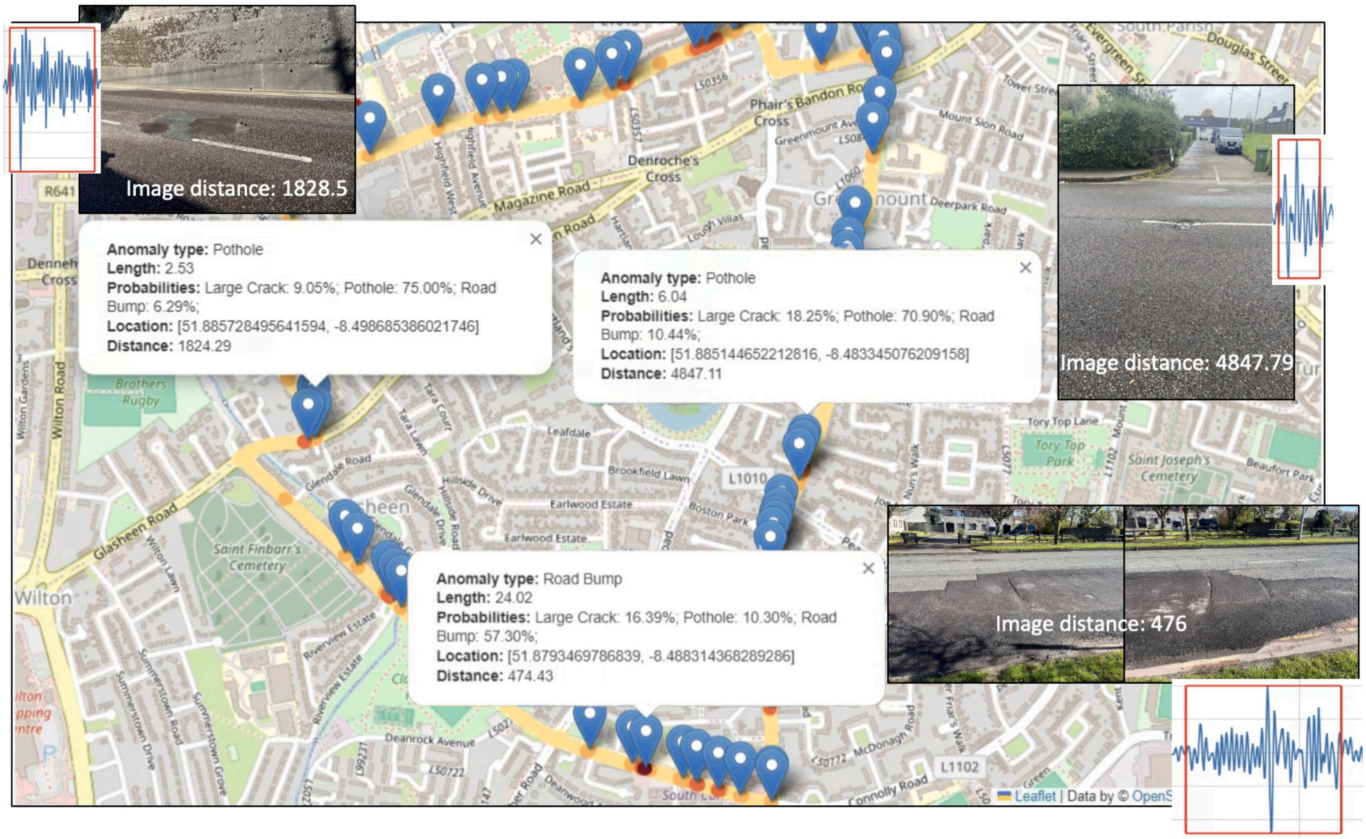

Fig. 15. Selected anomaly detection results by 2-stage ML system on Mercedes Sprinter Traveliner and validations by manual inspection.

derivations. This matches the length scales for the class of potholes, which are slender ratio, mean absolute, P2Pmax and standard derivation.

Table 3 also illustrates the overall importance of features to the entire model. For example, P2Pmax has small length scales on classes 1, 2 and 4, indicating a high connection to those classes. Meanwhile, SMA has high length scales across almost all classes, suggesting that this feature might have a limited impact on the GPC model if excluded during the training process.

The GPC, being a stochastic model, generates predictions based on the posterior distribution's mean and probability (covariance). The prediction probabilities provide insights into potential misclassification

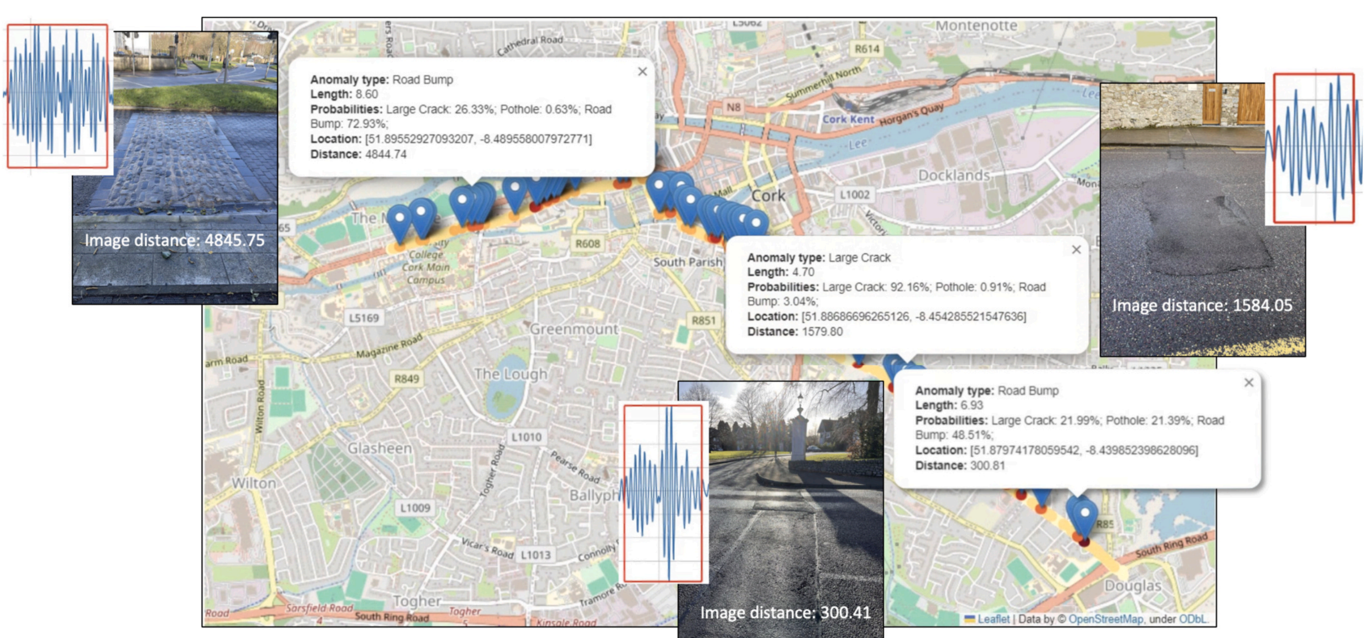

Fig. 16. Selected anomaly detection results by 2-stage ML system on Volvo B9 and validations by manual inspection.

errors. In some cases, the predictions can be ambiguous, where the maximum class probabilities are relatively low, making decision-making challenging. This could be due to either a region of strong overlap between classes, or a lack of training examples within this region, leading to high uncertainties, such as the bottom case shown in the Fig. 16. To reduce those uncertainties, one can simply add more samples located around the uncertainty regions. While adding an extensive number of labelled samples could address this issue, it comes with the trade-off of increased computational effort for both training and prediction in the GPC model due to its nonparametric nature.

Misclassifications can also arise when the vehicle intentionally avoids running over road anomalies labelled based on manual inspections. For instance, if drivers spot significant defects on the road, they might consciously steer clear of these anomalies. Consequently, the dataset may lack vibration data corresponding to these anomalies, leading to false positives in the predictions by the first stage model, thereby failing to be classified correctly by the second one. Correcting such errors is challenging, as these events are difficult to be recorded during data collection and, therefore, are absent from the labelled datasets. It is important to note that these errors are not intrinsic to the machine learning model itself. In essence, the GPC model could achieve greater accuracy if such errors were not present.

Given the limited dataset of the second stage machine learning model, a K-fold cross-validation was conducted to demonstrate the robustness of the model and minimize the variance in performance. The entire dataset was split into 5 folds, respectively. In each training iteration, one fold was used as the test set and the rest was used for the model training. The overall accuracy of the model consistently converged to approximately 87.39% with 0.0383 standard derivation. This convergence demonstrates the robustness of the machine learning model, affirming its suitability for application in road pavement anomaly detection.

In addition to road anomaly classification, supplementary information such as anomaly locations (extracted from data preprocessing), anomaly lengths (extracted from the first stage model), and the severity of defects (represented by the standard deviation of each anomaly window) can be provided. This additional information enhances decision-making processes for road maintenance. The details are visualized on an interactive map using OpenStreetMap. The results of two labelled routes are presented in the Figs. 15 and 16, where deeper red hues indicate the severity of road anomalies. Validations are conducted by manual inspection on each route, shown as images in Figs. 15 and 16, where locations of anomalies are extracted from image metadata.

6. Conclusions

This research introduces a structural health monitoring system framework with a two-stage machine learning approach for the detection and classification of road anomalies using smartphone motion sensors and GPS data at the community scale. In this framework, the first stage employs a Random Forest Classifier to identify potential anomalies, while the second stage utilizes a Gaussian Process Classifier for detailed classification.

The two-stage machine learning model outperforms the traditional machine learning model due to its capability of capturing the vibration events of anomalies without including redundant vibrations, thereby increasing the accuracy of features that describe the anomalies. On the other hand, the proposed methodology utilizes the geospatial series for the first time in the context of road anomaly detection. Compared with time series data, the geospatial series is time-independent, eliminating the effects of vehicles' speed of anomaly detections, thereby being suitable for complex driving environments.

Moreover, the study addresses challenges associated with noise reduction, sensor inaccuracies, and GPS errors in the preprocessing stages, ensuring the quality of the collected data. The application of filters, such as a Butterworth filter, effectively reduces noise from sources like engine vibrations and driver maneuver, contributing to the reliability of the subsequent machine learning models.

The developed two-stage model was evaluated on two representative road segments in Cork, Ireland. It demonstrates promising results, achieving robustness through cross-validation and exhibiting good performance across various fold splits. Despite challenges associated with potential misclassifications arising from drivers evading anomalies, the model's overall accuracy converges to approximately 87%, demonstrating its suitability for real-world applications.

The significance of this research extends beyond anomaly detection. The proposed methodology provides valuable supplementary information, including anomaly locations, lengths, and severity, which can be visualized on an interactive map. The proposed approach offers a more accurate and informative representation than traditional maps only incorporating local city council monitoring results.

As the geospatial series data is time-independent, the presented research did not consider the weakening effect of vibrations when vehicles run over anomalies at high speed. Therefore, the proposed methodology might misclassify some of the anomalies in such cases. In future research, the relationship between the intensity of vibrations of anomalies and the speed of testing vehicles will be investigated in order to enhance the model performance in a wider range of driving scenarios.

Current research using the two-stage model primarily focuses on detecting and classifying road pavement anomalies. Future studies will further extend the two-stage model to include road roughness estimation using the International Roughness Index in order to provide indicators of severity of road pavement deterioration, improving decision-making in road maintenance.

CRediT authorship contribution statement

Kai Zhao: Writing – original draft, Validation, Methodology, Investigation, Data curation. **Shuoshuo Xu:** Writing – review & editing, Software, Investigation, Data curation. **James Loney:** Resources, Funding acquisition, Conceptualization. **Andrea Visentin:** Writing – review & editing, Validation, Supervision, Investigation, Funding acquisition, Conceptualization. **Zili Li:** Writing – review & editing, Supervision, Methodology, Funding acquisition, Data curation, Conceptualization.

Declaration of competing interest

The authors declare that they have no known competing financial interests or personal relationships that could have appeared to influence the work reported in this paper.

Data availability

Data will be made available on request.

Acknowledgement

This publication has emanated from research conducted with the financial support of the EU Commission Recovery and Resilience Facility under the Science Foundation Ireland Future Digital Challenge Grant Number 22/NCF/FD/10932, and secondarily by SFI, Grant number 12/RC/2289-P2 co-funded under the European Regional Development Fund. For the purpose of Open Access, the author has applied a CC BY public copyright licence to any Author Accepted Manuscript version arising from this submission.

References

[1] A. Mednis, G. Strazdins, R. Zviedris, G. Kanonirs, L. Selavo, Real time pothole detection using Android smartphones with accelerometers, in: 2011 International Conference on Distributed Computing in Sensor Systems and Workshops, DCOSS'11, 2011, https://doi.org/10.1109/DCOSS.2011.5982206.

[2] J.W. Lim, T.T.V. Yap, V.T. Goh, H. Ng, W.J. Yap, T.Y. Kuek, Street SAFE - road fault monitoring and reporting, Int. J. Eng. Trends Technol. (2020) 120–124, https://doi.org/10.14445/22315381/CATI1P222.
[3] D. Dong, Z. Li, Smartphone sensing of road surface condition and defect detection, Sensors 21 (16) (2021) 5433, https://doi.org/10.3390/s21165433.
[4] Q. Yu, Y. Fang, R. Wix, Pavement roughness index estimation and anomaly detection using smartphones, Autom. Constr. 141 (2022) 104409, https://doi.org/10.1016/j.autcon.2022.104409.
[5] National Transportation Research Group, Bumpy Roads Ahead: America's Roughest Rides and Strategies to Make our Roads Smoother. https://tripnet.org/reports/bumpy-roads-ahead-americas-roughest-rides-and-strategies-to-make-our-roads-smooth/, 2023.
[6] Department of Transport of Ireland, Transport-Trends-2020 An Overview of Ireland's Transport Sector. https://www.gov.ie/pdf/?file=https://assets.gov.ie/124419/b6ea707f-c065-4943-ab29-d251cd0ff7a4.pdf#page=null, 2020.
[7] W. Li, M. Burrow, N. Metje, G. Ghataora, Automatic road survey by using vehicle mounted laser for road asset management, IEEE Access 8 (2020) 94643–94653, https://doi.org/10.1109/ACCESS.2020.2994470.
[8] J. Laurent, J.F. Hébert, D. Lefebvre, Y. Savard, Using 3D Laser Profiling Sensors for the Automated Measurement of Road Surface Conditions, 2012, pp. 157–167, https://doi.org/10.1007/978-94-007-4566-7_16.
[9] C. Koch, G.M. Jog, I. Brilakis, Automated pothole distress assessment using asphalt pavement video data, J. Comput. Civ. Eng. 27 (2013) 370–378, https://doi.org/10.1061/(asce)cp.1943-5487.0000232.
[10] J. Canny, A computational approach to edge detection, IEEE Trans. Pattern Anal. Mach. Intell. PAMI-8 (1986) 679–698, https://doi.org/10.1109/TPAMI.1986.4767851.
[11] S. Sattar, S. Li, M. Chapman, Road surface monitoring using smartphone sensors: a review, Sensors (Switzerland) 18 (2018) 3845, https://doi.org/10.3390/s18113845.
[12] R. Kumar, A. Mukherjee, V.P. Singh, Community sensor network for monitoring road roughness using smartphones, J. Comput. Civ. Eng. 31 (2017) 1–11, https://doi.org/10.1061/(asce)cp.1943-5487.0000624.
[13] F.S. Cabral, M. Pinto, F.A.L.N. Mouzinho, H. Fukai, S. Tamura, An automatic survey system for paved and unpaved road classification and road anomaly detection using smartphone sensor, in: Proceedings of the 2018 IEEE International Conference on Service Operations and Logistics, and Informatics, SOLI 2018, 2018, pp. 65–70, https://doi.org/10.1109/SOLI.2018.8476788.
[14] R. Du, G. Qiu, K. Gao, L. Hu, L. Liu, Abnormal road surface recognition based on smartphone acceleration sensor, Sensors (Switzerland) 20 (2020) 451, https://doi.org/10.3390/s20020451.
[15] V. Douangphachanh, H. Oneyama, Exploring the use of smartphone accelerometer and gyroscope to study on the estimation of road surface roughness condition, in: ICINCO 2014 - Proceedings of the 11th International Conference on Informatics in Control, Automation and Robotics 1, 2014, pp. 783–787, https://doi.org/10.5220/0005117407830787.
[16] A. Basavaraju, J. Du, F. Zhou, J. Ji, A machine learning approach to road surface anomaly assessment using smartphone sensors, IEEE Sensors J. 20 (2020) 2635–2647, https://doi.org/10.1109/JSEN.2019.2952857.
[17] K. Zang, J. Shen, H. Huang, M. Wan, J. Shi, Assessing and mapping of road surface roughness based on GPS and accelerometer sensors on bicycle-mounted smartphones, Sensors (Switzerland) 18 (2018) 914, https://doi.org/10.3390/s18030914.
[18] S. Sattar, S. Li, M. Chapman, Developing a near real-time road surface anomaly detection approach for road surface monitoring, Measurement (Lond) 185 (2021) 109990, https://doi.org/10.1016/j.measurement.2021.109990.
[19] R. Bhoraskar, N. Vankadhara, B. Raman, P. Kulkarni, Wolverine: Traffic and road condition estimation using smartphone sensors, in: 2012 4th International Conference on Communication Systems and Networks, COMSNETS 2012, 2012, pp. 1–6, https://doi.org/10.1109/COMSNETS.2012.6151382.
[20] H.W. Wang, C.H. Chen, D.Y. Cheng, C.H. Lin, C.C. Lo, A real-time pothole detection approach for intelligent transportation system, Math. Probl. Eng. 2015 (2015), https://doi.org/10.1155/2015/869627.
[21] G. Sebestyen, D. Muresan, A. Hangan, Road quality evaluation with mobile devices, in: Proceedings of the 2015 16th International Carpathian Control Conference, ICCC 2015, 2015, pp. 458–464, https://doi.org/10.1109/CarpathianCC.2015.7145123.
[22] P. Mohan, V.N. Padmanabhan, R. Ramjee, Nericell: Rich monitoring of road and traffic conditions using mobile smartphones, in: SenSys'08 - Proceedings of the 6th Association for Computing Machinery Conference on Embedded Networked Sensor Systems, 2008, pp. 323–336, https://doi.org/10.1145/1460412.1460444.
[23] K. Yagi, Extensional smartphone probe for road bump detection, in: 17th Intelligent Transport System World Congress, 2010, pp. 1–10. https://www.bumprecorder.com/wp-content/uploads/2013/12/225c966eb8450f15af993862b032ba6e.pdf.
[24] T. Nomura, Y. Shiraishi, A method for estimating road surface conditions with a smartphone, Int. J. Inform. Soc. 7 (2015) 29–36. http://www.infsoc.org/journal/vol07/IJIS_07_1_029-036.pdf.
[25] A. Vittorio, V. Rosolino, I. Teresa, C.M. Vittoria, P.G. Vincenzo, D.M. Francesco, Automated sensing system for monitoring of road surface quality by mobile devices, Procedia Soc. Behav. Sci. 111 (2014) 242–251, https://doi.org/10.1016/j.sbspro.2014.01.057.
[26] C.W. Yi, Y.T. Chuang, C.S. Nian, Toward crowdsourcing-based road pavement monitoring by mobile sensing technologies, IEEE Trans. Intell. Transp. Syst. 16 (2015) 1905–1917, https://doi.org/10.1109/TITS.2014.2378511.
[27] R. Du, G. Qiu, K. Gao, L. Hu, L. Liu, Abnormal road surface recognition based on smartphone acceleration sensor, Sensors (Switzerland) 20 (2020) 451, https://doi.org/10.3390/s20020451.
[28] M.Y. Alam, A. Nandi, A. Kumar, S. Saha, M. Saha, S. Nandi, S. Chakraborty, Crowdsourcing from the true crowd: device, vehicle, road-surface and driving independent road profiling from smartphone sensors, Pervasive Mobile Comput. 61 (2020) 101103, https://doi.org/10.1016/j.pmcj.2019.101103.
[29] M. Perttunen, O. Mazhelis, F. Cong, M. Kauppila, T. Leppänen, J. Kantola, J. Collin, S. Pirttikangas, J. Haverinen, T. Ristaniemi, J. Riekki, Distributed road surface condition monitoring using mobile phones, in: Lecture Notes in Computer Science (Including Subseries Lecture Notes in Artificial Intelligence and Lecture Notes in Bioinformatics) 6905 LNCS, 2011, pp. 64–78, https://doi.org/10.1007/978-3-642-23641-9_8.
[30] K. Pawar, S. Jagtap, S. Bhoir, Efficient pothole detection using smartphone sensors, ITM Web Conf. 32 (2020) 03013, https://doi.org/10.1051/itmconf/20203203013.
[31] M.R. Dey, U. Satapathy, P. Bhanse, B.K. Mohanta, D. Jena, MagTrack: Detecting Road Surface Condition using Smartphone Sensors and Machine Learning, IEEE Region 10 Annual International Conference, Proceedings/TENCON 2019-Octob, 2019, pp. 2485–2489, https://doi.org/10.1109/TENCON.2019.8929717.
[32] N. Silva, J. Soares, V. Shah, M.Y. Santos, H. Rodrigues, Anomaly detection in roads with a data mining approach, Procedia Comput. Sci. 121 (2017) 415–422, https://doi.org/10.1016/j.procs.2017.11.056.
[33] Y.C. Tai, C.W. Chan, J.Y. Hsu, Automatic road anomaly detection using smart mobile device, in: Conference on Technologies and Applications of Artificial Intelligence, 2010. https://citeseerx.ist.psu.edu/document?repid=rep1&type=pdf&doi=0669241928cbdf9f847075db299cdd467a6345f2.
[34] H. Maeda, Y. Sekimoto, T. Seto, T. Kashiyama, H. Omata, Road Damage Detection Using Deep Neural Networks with Images Captured Through a Smartphone 2000, 2018, pp. 4–6, https://doi.org/10.1111/mice.12387.
[35] B. Varona, A. Monteserin, A. Teyseyre, A deep learning approach to automatic road surface monitoring and pothole detection, Pers. Ubiquit. Comput. 24 (2020) 519–534, https://doi.org/10.1007/s00779-019-01234-z.
[36] T.Y. Chuang, N.H. Perng, J.Y. Han, Pavement performance monitoring and anomaly recognition based on crowdsourcing spatiotemporal data, Autom. Constr. 106 (2019) 102882, https://doi.org/10.1016/j.autcon.2019.102882.
[37] I. Ferjani, S.A. Alsaif, How to get best predictions for road monitoring using machine learning techniques, PeerJ Comput. Sci. 8 (2022), https://doi.org/10.7717/PEERJ-CS.941.
[38] S. Sattar, A Crowdsourcing Technique For Road Surface Monitoring Using Smarthphone Sensors, Toronto Metropolitan University, 2021, https://doi.org/10.32920/ryerson.14655333.v1. Ph.D. Dissertation.